JACS
JOURNAL OF THE AMERICAN CHEMICAL SOCIETY

Subscriber access provided by American Chemical Society

Article

Activation of High-*T* Ferromagnetism in Co:TiO and Cr:TiO Nanorods and Nanocrystals by Grain Boundary Defects

J. Daniel Bryan, Steven A. Santangelo, Sean C. Keveren, and Daniel R. Gamelin

J. Am. Chem. Soc., **2005**, 127 (44), 15568-15574• DOI: 10.1021/ja0543447 • Publication Date (Web): 18 October 2005

Downloaded from http://pubs.acs.org on March 25, 2009

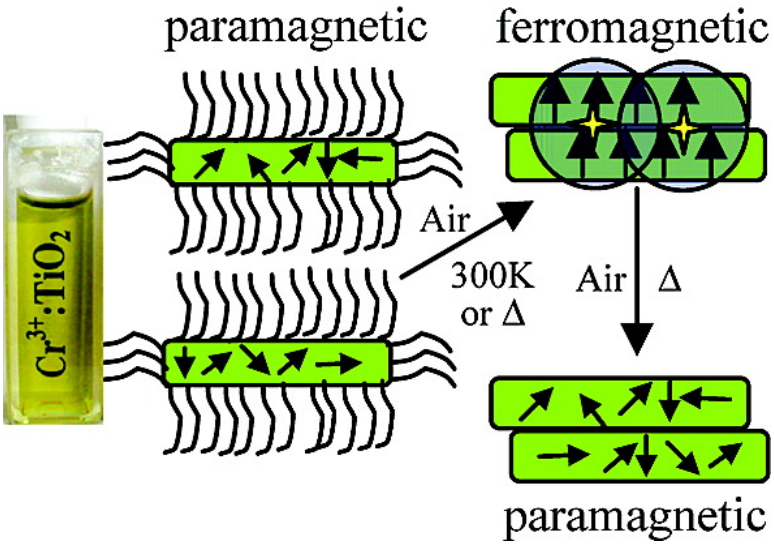

More About This Article

Additional resources and features associated with this article are available within the HTML version:

- Supporting Information
- Links to the 14 articles that cite this article, as of the time of this article download
- Access to high resolution figures
- Links to articles and content related to this article
- Copyright permission to reproduce figures and/or text from this article

View the Full Text HTML

ACS Publications
High quality. High impact.

Journal of the American Chemical Society is published by the American Chemical Society. 1155 Sixteenth Street N.W., Washington, DC 20036

J|A|C|S
ARTICLES
Published on Web 10/18/2005

Activation of High-T_C Ferromagnetism in Co^{2+}:TiO_2 and Cr^{3+}:TiO_2 Nanorods and Nanocrystals by Grain Boundary Defects

J. Daniel Bryan, Steven A. Santangelo, Sean C. Keveren, and Daniel R. Gamelin*

Contribution from the Department of Chemistry, University of Washington, Seattle, Washington 98195-1700

Received June 30, 2005; E-mail: Gamelin@chem.washington.edu

Abstract: Colloidal Co^{2+}- and Cr^{3+}-doped TiO_2 nanorods and nanocrystals were synthesized and studied by X-ray powder diffraction, electronic absorption spectroscopy, magnetic circular dichroism spectroscopy, magnetic susceptibility, and transmission electron microscopy. The nanorods were paramagnetic as colloids but showed room-temperature ferromagnetism when spin-coated aerobically into films. Crystalline domain size, thermal annealing, and dopant or defect migration are not the dominating factors converting the doped TiO_2 nanocrystals from the paramagnetic state to the ferromagnetic state. The most important factor for activating ferromagnetism is found to be the creation of grain boundary defects, proposed to be oxygen vacancies at nanocrystal fusion interfaces. These defects are passivated and the ferromagnetism destroyed by further aerobic annealing. These results not only help elucidate the origins of the TM^{n+}:TiO_2 DMS ferromagnetism but also represent an advance toward the controlled manipulation of high-T_C DMS ferromagnetism using external chemical perturbations.

I. Introduction

Ferromagnetic diluted magnetic semiconductors (DMS) with Curie temperatures (T_C) above room temperature are essential components of many of the proposed room-temperature spin-based electronics (spintronics) devices.[1] Device miniaturization has made manipulating ferromagnetism on the nanoscale using epitaxially deposited[2] or colloidal DMS quantum dots[3] a goal of considerable interest.[4] The discovery of high-T_C ferromagnetism in 2% Co^{2+}:TiO_2 anatase thin films by Matsumoto et al.[5] sparked a tremendous experimental and theoretical research effort focused on understanding the ferromagnetism of this doped metal oxide. Several researchers attempted to explain this surprising observation by showing that dopant ion segregation and reduction can form ferromagnetic precipitates under certain growth conditions and that ferromagnetism in doped TiO_2 was therefore likely not intrinsic.[6] Other groups have reported ferromagnetism in the absence of such precipitates.[7−11] Our group's work involving colloidal Co^{2+}:TiO_2 nanocrystals prepared by direct chemical routes using oxidized ionic precursors has shown that ferromagnetic samples with large ferromagnetic saturation moments (M_s up to 1.9 μ_B/Co^{2+} in 3% Co^{2+}:TiO_2) can be prepared under oxidative conditions that preclude the formation of cobalt metal, strongly supporting the existence of intrinsic DMS ferromagnetism in nonstoichiometric Co^{2+}:$TiO_{2-\delta}$.[12] High-T_C ferromagnetism in dilute doped metal oxides is now generally considered to be an intrinsic phenomenon,[13,14] and fundamental questions concerning the microscopic origins of this ferromagnetism must now be addressed.

In this paper, we describe a series of experiments designed to investigate the conversion from paramagnetic to ferromagnetic phases in nanocrystalline TM^{n+}:TiO_2 (TM^{n+} = Co^{2+} and Cr^{3+}) prepared by direct chemical routes. This chemical approach was shown previously to yield some of the largest saturation moments to date for any TiO_2 DMS.[12] Three hypotheses were considered to explain the observation that free-standing

(1) Awschalom, D. D.; Flatté, M. E.; Samarth, N. *Sci. Am.* **2002**, *286*, 66.
(2) Bacher, G.; Schoemig, H.; Scheibner, M.; Forchel, A.; Maksimov, A. A.; Chernenko, A. V.; Dorozhkin, P. S.; Kulakovskii, V. D.; Kennedy, T.; Reinecke, T. L. *Physica E* **2005**, *26*, 37; Lee, S.; Dobrowolska, M.; Furdyna, J. K. *Physica E* **2005**, *26*, 271.
(3) Bryan, J. D.; Gamelin, D. R. *Prog. Inorg. Chem.* **2005**, *54*, 47.
(4) Efros, A. L.; Rashba, E. I.; Rosen, M. *Phys. Rev. Lett.* **2001**, *87*, 206601.
(5) Matsumoto, Y.; Murakami, M.; Shono, T.; Hasegawa, T.; Fukumura, T.; Kawasaki, M.; Ahmet, P.; Chikyow, T.; Koshihara, S.; Koinuma, H. *Science* **2001**, *291*, 854.
(6) Kim, D. H.; Yang, J. S.; Lee, K. W.; Bu, S. D.; Noh, T. W.; Oh, S. J.; Kim, Y. W.; Chung, J. S.; Tanaka, H.; Lee, H. Y.; Kawai, T. *Appl. Phys. Lett.* **2002**, *81*, 2421; Kim, J. Y.; Park, J. H.; Park, B. G.; Noh, H. J.; Oh, S. J.; Yang, J. S.; Kim, D. H.; Bu, S. D.; Noh, T. W.; Lin, H. J.; Hsieh, H. H.; Chen, C. T. *Phys. Rev. Lett.* **2003**, *90*, 017401.
(7) Chambers, S. A.; Droubay, T.; Wang, C. M.; Lea, A. S.; Farrow, R. F. C.; Folks, L.; Deline, V.; Anders, S. *Appl. Phys. Lett.* **2003**, *82*, 1257.
(8) Chambers, S. A.; Heald, S. M.; Droubay, T. *Phys. Rev. B.* **2003**, *67*, 100401; Chambers, S. A.; Thevuthasan, S.; Farrow, R. F. C.; Marks, R. F.; Thiele, J. U.; Folks, L.; Samant, M. G.; Kellock, A. J.; Ruzycki, N.; Ederer, D. L.; Diebold, U. *App. Phys. Lett.* **2001**, *79*, 3467.
(9) Griffin, K. A.; Pakomov, A. B.; Wang, C. M.; Heald, S. M.; Krishnan, K. M. *Phys. Rev. Lett.* **2005**, *94*, 157204.
(10) Toyosaki, H.; Fukumura, T.; Yamada, Y.; Kawasaki, M. *Appl. Phys. Lett.* **2005**, *86*, 182503.
(11) Jaffe, J. E.; Droubay, T. C.; Chambers, S. A. *J. Appl. Phys.* **2005**, *97*, 073908.
(12) Bryan, J. D.; Heald, S. M.; Chambers, S. A.; Gamelin, D. R. *J. Am. Chem. Soc.* **2004**, *126*, 11640.
(13) Pearton, S. J.; Heo, W. H.; Ivill, M.; Norton, D. P.; Steiner, T. *Semicond. Sci. Technol.* **2004**, *19*, R59; Chambers, S. A.; Droubay, T. C.; Kaspar, T. C. Epitaxial Growth and Properties of Magnetically Doped TiO_2. In *Thin Films and Heterostructures for Oxide Electronics*; Ogale, S. B., Ed.; Springer: New York, 2005.
(14) Coey, J. M. D.; Venkatesan, M.; Fitzgerald, C. B. *Nat. Mater.* **2005**, *4*, 173.

10.1021/ja0543447 CCC: $30.25 © 2005 American Chemical Society

Co^{2+}:TiO_2 nanocrystals were paramagnetic (not superparamagnetic), whereas spin-coated films of the same nanocrystals were strongly ferromagnetic: (1) Ferromagnetism in TM^{n+}:TiO_2 requires an electronically coupled domain that is sufficiently large to involve a critical number of dopants. Once that critical domain size is reached, ferromagnetism is thermodynamically favorable. (2) A thermal activation barrier must be overcome that was not reached at the low temperatures used to synthesize the TM^{n+}:TiO_2 colloids, perhaps related to dopant or defect migration. (3) The ferromagnetism is activated by formation of donor-like defects at DMS grain boundaries, in this case at nanocrystal fusion interfaces, and these defects mediate long-range magnetic exchange coupling. With the use of colloidal TM^{n+}:TiO_2 nanorods ($TM^{n+} = Co^{2+}$ or Cr^{3+}) prepared by direct chemical synthesis, these three hypotheses have been systematically tested and hypotheses (1) and (2) have been ruled out. Data attesting to the important role played by grain boundary defects is presented, and the dependence of ferromagnetism on such defects found here is discussed in the context of current models for ferromagnetism in oxide DMSs.

II. Experimental Section

II.A. Sample Preparation. The synthesis of Co^{2+}:TiO_2 and Cr^{3+}:TiO_2 nanorods was adapted from a low-temperature hydrolytic route shown to yield colloidal crystalline nanorods.[15] In a typical Co^{2+}:TiO_2 nanorod synthesis, 160 mL of oleic acid (OA, Aldrich tech grade 90%) was combined with 0.35 g of cobalt (II) acetate tetrahydrate in a three-neck flask under vigorous stirring and degassed under vacuum at 115 °C. The flask was cooled to 100 °C and placed under a N_2 environment. At 100 °C, 6 mL of titanium (IV) tetraisopropoxide (99% Strem, Ti(*i*-OPr)$_4$) was injected into the flask using a gastight syringe employing standard air-free techniques. The reaction was allowed to stir for 5−10 min, after which 6 mL of 2 M trimethylamine *N*-oxide dihydrate (98% Avacodo Research Chemicals) was injected into the flask, causing an abrupt drop in temperature to 80−85 °C. The reaction was reheated to 100 °C and allowed to stir for 12 h under a gentle reflux. Excess water was removed under vacuum. The precipitate was separated from the mother liquor by centrifugation and dissolved readily into toluene. Excess OA was removed by repeated washing steps involving precipitation with absolute ethanol followed by re-suspension in toluene to yield high optical quality colloidal suspensions. Preparation of Cr^{3+}:TiO_2 nanorods followed the same procedure, substituting chromium (III) acetate monohydrate (99% Matheson) for the cobalt precursor.

II.B. Postsynthetic Processing. The surface-capping ligand was changed to trioctylphosphine oxide (TOPO, 90% tech grade Aldrich) by heating the precipitated nanorods in excess TOPO at 180 °C for several minutes. Time-dependent colloid-annealing experiments were performed by raising the temperature of the degassed TOPO/nanorod suspension up to 250, 300, or 320 °C under inert atmosphere. Aliquots were removed at various times and rapidly cooled to room temperature where they formed waxy solids. The waxy solids were soluble in toluene and were washed repeatedly using the previously mentioned procedure to remove excess TOPO. Thin films were made by spin coating the OA- or TOPO-capped colloids from toluene followed by aerobic annealing at 350 °C between each coat. Unless otherwise specified, the annealing time for each coat was 1 min. Gentle Soxhlet extractions were performed on precipitated powders using absolute ethanol and a Soxhlet extraction apparatus under aerobic conditions (3 days) to remove the OA ligands. The ethanol condensate washing the nanorod powders in the Soxhlet apparatus was approximately room temperature.

(15) Cozzoli, P. D.; Kornowski, A.; Weller, H. *J. Am. Chem. Soc.* **2003**, *125*, 14539.

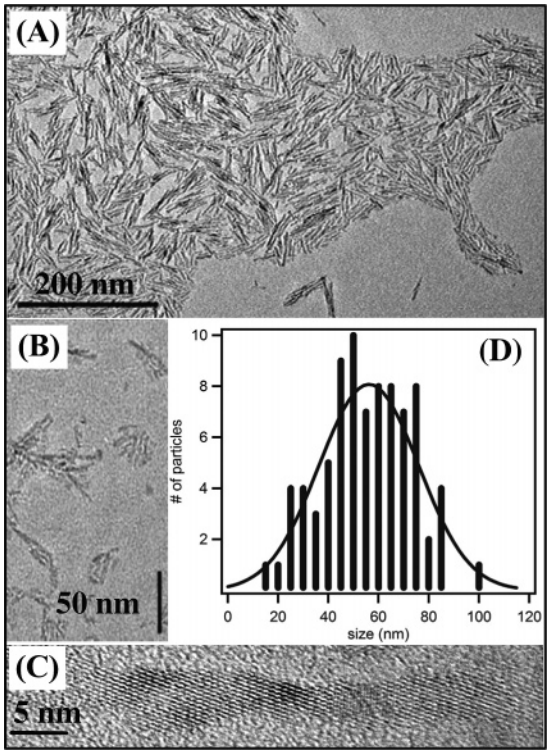

Figure 1. Overview TEM images of (A) 4.0% Co^{2+}:TiO_2 and (B) 1.4% Cr^{3+}:TiO_2 nanorods. (C) High-resolution image of a 4.0% Co^{2+}:TiO_2 nanorod. (D) Histogram showing distribution of Co^{2+}:TiO_2 nanorod lengths.

II.C. Physical Methods. High-resolution transmission electron microscopy (TEM) images were collected at the Pacific Northwest National Laboratory on a JEOL 2010 (200 kV) microscope with a high-brightness LaB_6 filament electron source. X-ray powder diffraction (XRD) data for nanocrystals precipitated from toluene were collected on an 800 W Philips 1830 powder diffractometer using an etched glass plate sample holder. Dopant concentrations were measured by inductively coupled plasma atomic emission spectroscopy (ICP-AES, Jarrel-Ash model 955) using elemental calibration standards (High Purity Standards). Thermogravimetric data were collected under flowing air using a TA Instruments model Q50. Electronic absorption spectra were collected on a Cary 5E (Varian) spectrophotometer using 1 cm path length quartz cuvettes. Magnetic circular dichroism (MCD) spectra were collected using a UV−vis−NIR MCD instrument constructed from an AVIV 40DS spectropolarimeter and a high-field superconducting magnetooptical cryostat (Cryo-Industries SMC-1659 OVT) with a variable temperature sample compartment positioned in the Faraday configuration. Magnetic susceptibilities were measured using a Quantum Design Magnetic Property Measurement System equipped with a reciprocating sample option. All thin film and powder magnetization data were corrected for diamagnetism of the substrate and/or sample holder.

III. Results

Figures 1 and 2 show representative TEM and XRD data collected for Co^{2+}:TiO_2 and Cr^{3+}:TiO_2 nanorods. The pronounced shape anisotropy observed by TEM and the narrow (004) reflection present in the $I4_1/amd$ space group of anatase indicates that the *c*-axis of the nanorods is parallel to the growth direction.[15] Figure 1D shows a distribution of nanorod lengths obtained by analyzing >100 nanorods from several TEM images. Analysis shows an average rod length of 56 ± 19 nm. Although the nanorods varied substantially in length, the vast majority had thicknesses of 5−7 nm (Figure 1C). In addition,

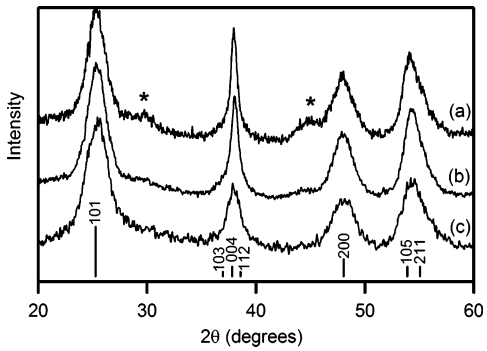

Figure 2. X-ray powder diffraction of (a) oleic-acid-capped 1.4% Cr^{3+}:TiO_2 nanorods, (b) oleic-acid-capped 4.0% Co^{2+}:TiO_2 nanorods, (c) TOPO-capped 3.0% Co^{2+}:TiO_2 TOPO nanocrystals. The reference reflections for bulk TiO_2 anatase are also included. ∗ indicates reflections from close packed capping ligands.

many of the nanorods showed bifurcation and twinning patterns consistent with the "oriented attachment" mechanism of rod growth elucidated previously for TiO_2 anatase nanoparticles and nanorods.[16,17]

Figure 3 shows 300 K electronic absorption spectra and 5 K, 0−6 T variable field MCD spectra of Cr^{3+}:TiO_2 nanorods. A partially resolved absorption feature centered at 16 400 cm^{-1} is observed along with rising absorbance to higher energy. The 16 400 cm^{-1} absorption band correlates to a structured feature in the 5 K MCD spectra (Figure 3B) at the same energy. The 5 K MCD spectra also show two narrow transitions at 13 441 cm^{-1} and 14 006 cm^{-1} overlapping the low-energy side of the 16 400 cm^{-1} feature. To higher energy, an intense negative MCD feature at 23 250 cm^{-1} was also observed.

The spectroscopic properties of the Co^{2+}:TiO_2 nanorods were indistinguishable from those of the Co^{2+}:TiO_2 spherical nanocrystals that were characterized in detail previously[12] (see the Supporting Information). Both displayed the same tan-brown color and broad absorption feature tailing into the visible energy region. MCD measurements in combination with ligand field calculations were used previously to demonstrate substitution of Co^{2+} onto the 6-coordinate Ti^{4+} D_{2d} sites in the anatase lattice.

Figure 4 shows effective magnetic moments (μ_{eff}) of OA-capped 4.0% Co^{2+}:TiO_2 and 1.4% Cr^{3+}:TiO_2 nanorods under a 5000 Oe applied field plotted as μ_B/TM^{n+} versus temperature ($TM^{n+} = Cr^{3+}$ or Co^{2+}). The μ_{eff} for the Cr^{3+}:TiO_2 nanorods is nearly temperature independent between 300 and 40 K at a value of 3.8 μ_B/Cr^{3+}. Similarly, μ_{eff} for Co^{2+}:TiO_2 is nearly temperature independent between 300 and 100 K at a value of 4.15 μ_B/Co^{2+}.

Figure 5 shows 300 K magnetization data for thin films cast from colloidal suspensions of 3.0% Co^{2+}:TiO_2 and 1.4% Cr^{3+}:TiO_2 nanorods along with films cast from 3.0% Co^{2+}:TiO_2 spherical nanocrystals.[12] None of these TiO_2 colloids were annealed prior to spin coating. The 300 K ferromagnetic saturation moment (M_s(300 K)) for the Co^{2+}:TiO_2 nanorod film (Figure 5A) is 0.069 μ_B/Co^{2+} with a coercive field of 95 Oe and remnant magnetization of 0.008 μ_B/Co^{2+}. The saturation moment for the Cr^{3+}:TiO_2 nanorod film (Figure 5B) is 0.12 μ_B/Cr^{3+} with a coercive field of 72 Oe and remnant magnetization 0.001 μ_B/Cr^{3+}. The average M_s(300 K) value of films prepared from the same nanorod synthesis batch is 0.069 ± 0.002 for Co^{2+}:TiO_2 (four films) and 0.12 ± 0.01 for Cr^{3+}:TiO_2 (three films). Figure 5C shows the 300 K saturation magnetization of three spin-coated thin films made from spherical Co^{2+}:TiO_2 nanocrystals. The films showed much larger

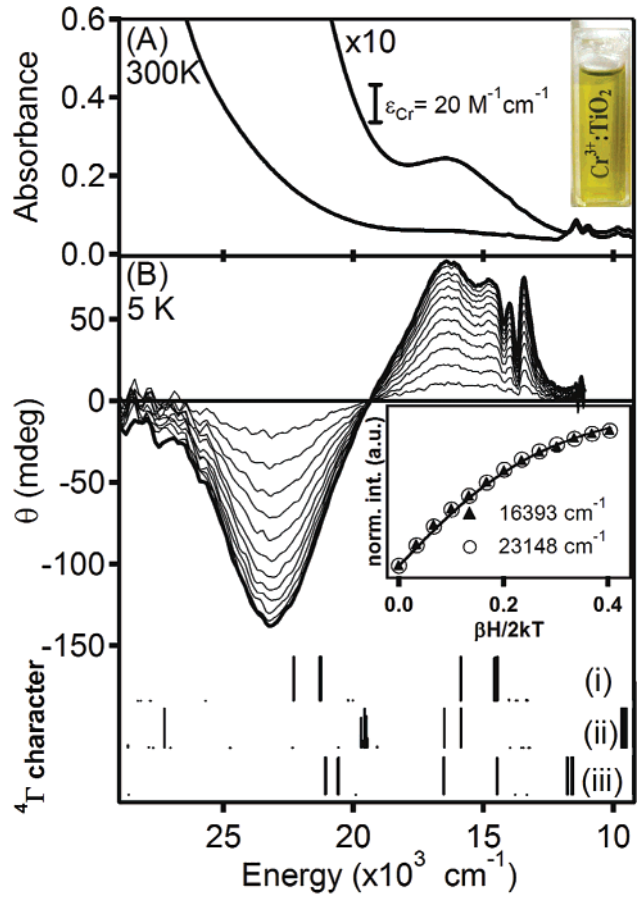

Figure 3. (A) Absorption spectra at 300 K of colloidal 1.4% Cr^{3+}:TiO_2 nanorods at different concentrations, suspended in toluene (inset). (B) MCD spectra at 5 K, 0−6 T, of a frozen solution of 1.4% Cr^{3+}:TiO_2 nanorods. Inset: Variable field MCD saturation magnetization at 5 K for the 16 400 and 23 150 cm^{-1} bands, fitted to eq 1 (solid line). Predicted energies of the ligand field transitions of Cr^{3+} in the D_{2d} anatase cation site with (i) 6-coordinate, (ii) 5-coordinate axial vacancy, and (iii) 5-coordinate equatorial vacancy geometries. See text for details.

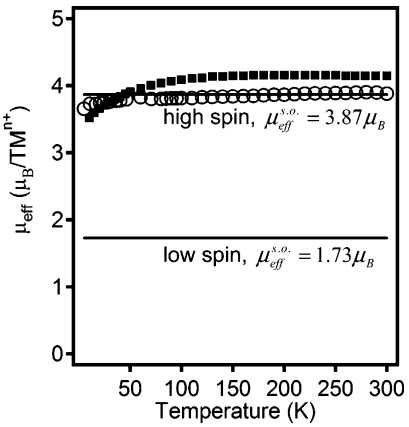

Figure 4. Temperature dependence of the effective magnetic moment per transition metal ion for 4.0% Co^{2+}:TiO_2 (■) and 1.4% Cr^{3+}:TiO_2 (○) nanorods. Spin-only effective magnetic moments for $S = 1/2$ and $S = 3/2$ are shown as solid lines for reference.

(16) Adachi, M.; Murata, Y.; Takao, J.; Jiu, J.; Sakamoto, M.; Wang, F. *J. Am. Chem. Soc.* **2004**, *126*, 14943.
(17) Zhang, H.; Banfield, J. F. *Chem. Mater.* **2002**, *14*, 4145.

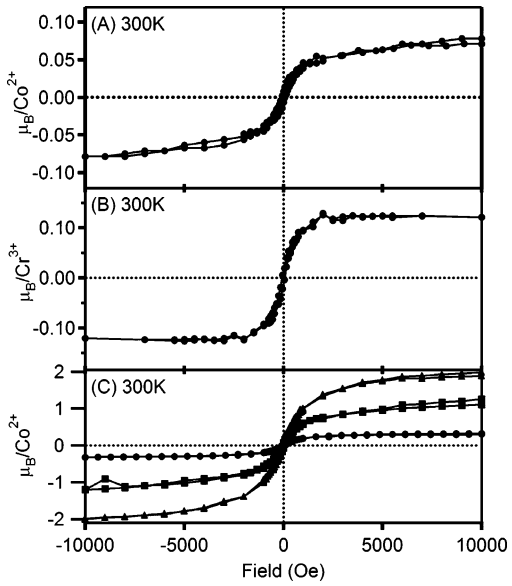

Figure 5. Magnetization data at 300 K collected on spin-coated films of (A) 3.0% Co^{2+}:TiO_2 nanorods, (B) 1.4% Cr^{3+}:TiO_2 nanorods, and (C) 3.0% Co^{2+}:TiO_2 spherical nanocrystals.

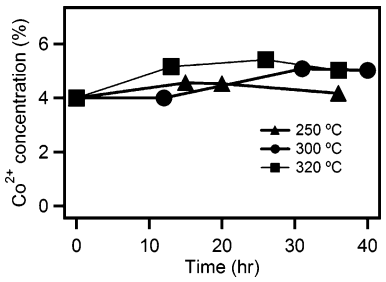

Figure 6. Co^{2+} concentrations in Co^{2+}:TiO_2 nanorods determined by ICP-AES, plotted vs annealing time at various temperatures. Error bars are approximately equal to the size of the data points.

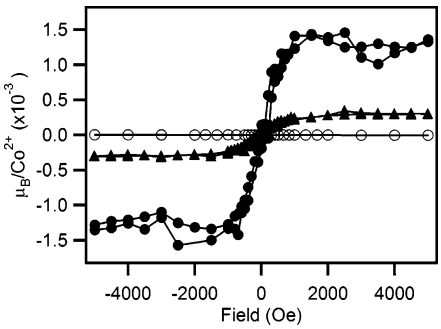

Figure 7. Magnetization at 300 K of (○) colloidal 4.0% Co^{2+}:TiO_2 nanorods annealed for 40 h at 320 °C in TOPO then resuspended in toluene, (▲) aggregated 4.0% Co^{2+}:TiO_2 nanorods, and (●) aggregated 3.0% Co^{2+}:TiO_2 spherical nanocrystals.

300 K saturation moments of 0.3, 1.0, and 1.9 μ_B/Co^{2+} (M_s-(avg) = 1.0 ± 0.8), coercive fields of 55, 47, and 55 Oe, and remnant fields of 0.02, 0.08, and 0.09 μ_B/Co^{2+}, respectively.

Figure 6 plots the analytical Co^{2+} concentrations in colloidal Co^{2+}:TiO_2 nanorods versus annealing time in pure TOPO at 250, 300, and 320 °C (the highest temperature achievable without solvent decomposition under the conditions used).

Figure 7 shows 300 K magnetization data for a colloidal suspension of 4.0% Co^{2+}:TiO_2 nanorods after solvent annealing at 320 °C for 40 h and for a powder sample of 4.0% Co^{2+}:TiO_2 nanorods from which the OA-capping ligands have

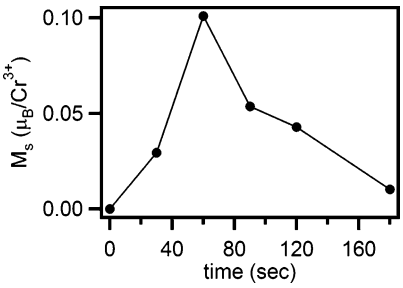

Figure 8. Ferromagnetic saturation moments at 300 K for thin films made from 1.4% Cr^{3+}:TiO_2 nanorods plotted vs annealing time at 350 °C between coats. All films were made using five coats deposited from the same stock suspension.

been removed by ∼25 °C Soxhlet extraction. The colloids showed no evidence of magnetic ordering whatsoever. A weak ferromagnetism (∼0.0003 μ_B/Co^{2+}) was observed in the aggregated 4.0% Co^{2+}:TiO_2 nanorods, approximately a factor of 5 smaller than that seen for aggregated spherical 3.0% Co^{2+}:TiO_2 nanocrystals (∼0.0015 μ_B/Co^{2+}).[12]

Figure 8 plots M_S(300 K) versus annealing times at 350 °C for a series of spin-coated 1.4% Cr^{3+}:TiO_2 thin films all prepared under identical aerobic conditions from the same colloidal suspension. A sharp rise in M_S(300 K) is observed from 0 to 60 s (slope ≈ 2×10^{-3} μ_B/Cr^{3+}/s) annealing time followed by a slower decrease from 60 to 180 s (slope ≈ -7×10^{-4} μ_B/Cr^{3+}/s).

IV. Analysis and Discussion

IV.A. Synthesis. The coordination number of Co^{2+} ions dissolved in OA changes from 6 to 4 upon dehydration of the Co^{2+}/OA mixture under dynamic vacuum at 140 °C, as indicated by a rose to purple color change. Injection of the titanium precursor into the dehydrated Co^{2+}/OA solution causes a purple to tan color change coinciding with a change in coordination environment from 4 to 6. This same color change was observed previously during the conversion of an amorphous purple Co^{2+}/Ti^{4+} oxo-oligomeric gel prepared at room temperature into tan Co^{2+}:TiO_2 colloidal nanocrystals by autoclaving.[12] For the nanorods, the elevated synthesis temperature (100 °C) is evidently sufficient to convert the 4-coordinate Co^{2+}/OA precursor into a 6-coordinate $(-Co-O-Ti-)_x$ species resulting in the purple to tan color change. Little or no color change was observed upon dehydration of the green Cr^{3+}/OA solution or upon injection of the Ti precursor into the Cr^{3+}/OA solution, indicating the coordination number is not changing during these steps. This preference of Cr^{3+} for a 6-coordinate geometry over the 4-coordinate geometry seen for Co^{2+} arises from the large ligand field stabilization energy (LFSE) of the d^3 configuration.[18] Since the LFSE for Co^{2+} is much smaller than for Cr^{3+}, Co^{2+} is easily interconverted thermally or chemically between 6- and 4-coordinate geometries, as evidenced by the color changes.

IV.B. Dopant Speciation in the Host Lattice. The close spectroscopic and magnetic similarity of the Co^{2+}:TiO_2 nanorods and the Co^{2+}:TiO_2 nanocrystals described previously[12] leads to the conclusion that the Co^{2+} ions occupy the same D_{2d} distorted Ti^{4+} cation site of anatase in the nanorods as in the nanocrystals. We therefore focus here on characterization and analysis of the chromium speciation in chromium-doped TiO_2. The absorption

(18) Huheey, J. E.; Keiter, E. A.; Keiter, R. L. *Inorganic Chemistry: Principles of Structure and Reactivity*; Harper Collins: Hinsdale, IL, 1993.

feature in Figure 3A centered at 16 400 cm^{-1} coincides with the intense positive MCD band at the same energy and is readily identified as the $^4A_2 \rightarrow {}^4T_2(F)$ ligand field transition of pseudo-octahedral Cr^{3+}. The increased ϵ value for this transition ($\epsilon(Cr^{3+}) = 27\ M^{-1}\ cm^{-1}$) over that of octahedral $Cr(H_2O)_6{}^{3+}$ ($\epsilon(Cr^{3+}) = 14\ M^{-1}\ cm^{-1}$)[19] is consistent with relaxation of the parity selection rule through the loss of inversion symmetry when changing from O_h to D_{2d} symmetry and provides support for the conclusion that Cr^{3+} substitutes onto the Ti^{4+} D_{2d} site. To higher energy, the rising absorption feature tailing into the ultraviolet arises from a combination of the higher energy $^4A_2 \rightarrow {}^4T_1(F)$ Cr^{3+} transition, clearly observed by MCD spectroscopy at 23 150 cm^{-1}, and a charge-transfer transition between the anatase host and the Cr^{3+} dopant ion. Diluting the sample by a factor of 10 (Figure 3A) failed to reveal any distinct shoulder in this rising absorption tail. The two weak absorption features centered at 13 441 and 14 006 cm^{-1} lying on the low-energy side of the 16 400 cm^{-1} band are assigned as the spin-forbidden $^4A_2 \rightarrow {}^2E$ and $^4A_2 \rightarrow {}^2T_2$ transitions. These spin-forbidden transitions are readily identified in the MCD spectra shown in Figure 3B at the same energies. The $^4A_2$ ground state is confirmed by the close fit of the MCD saturation magnetization data (Figure 3B) to the spin-only Brillouin function described by eq 1 using $S = 3/2$ and the g value of Cr^{3+} in TiO_2 rutile ($g = 1.98$),[20] where N, β, and k are constants, T is the temperature, and H is the applied magnetic field.

$$M_S = \frac{1}{2}Ng\beta\left((2S+1)\coth\left((2S+1)\left(\frac{g\beta H}{2kT}\right)\right) - \coth\left(\frac{g\beta H}{2kT}\right)\right) \quad (1)$$

The conclusion of substitutional Cr^{3+} doping is supported by energy level calculations in the angular overlap model[21] using ligand field parameters extrapolated from $Cr(H_2O)_6{}^{3+}$ ($10Dq = 17\ 400\ cm^{-1}$, $B = 695\ cm^{-1}$, $C = 4B$, and $\lambda = 197\ cm^{-1}$)[19,22] approximating the oxygen ligands as purely σ donors. Figure 3B shows the results of energy level calculations for Cr^{3+} substituting at the Ti^{4+} site with three different coordination environments: (i) 6-coordinate Cr^{3+}, (ii) 5-coordinate Cr^{3+} with an axial oxygen missing, and (iii) 5-coordinate Cr^{3+} with an equatorial oxygen missing. Ligand field transition intensities are represented as the $^4\Gamma$ character of the excited state wave function. Only the energies calculated for 6-coordinate Cr^{3+} agree well with the data. Importantly, this analysis demonstrates that charge compensation does not involve the loss of oxo anions in the first coordination sphere of the Cr^{3+} dopants.

The $S = 3/2$ ground states of Cr^{3+} and Co^{2+} are verified by quantitative variable temperature magnetic data collected on the isolated Co^{2+}:TiO_2 and Cr^{3+}:TiO_2 nanorods (Figure 4). The effective magnetic moment (μ_{eff}) for the Cr^{3+}:TiO_2 nanorods is nearly temperature independent between 300 and 40 K at a value of 3.8 μ_B/Cr^{3+}, very close to the spin-only value predicted for a $S = 3/2$ ion (3.87 μ_B/Cr^{3+}). The close adherence to the spin-only effective magnetic moment is a direct result of the absence of orbital angular momentum in the $^4A_2$ ground state of Cr^{3+}, and the quantitative agreement indicates all Cr^{3+} are accounted for as isolated paramagnetic ions. This latter result demonstrates that charge compensation does not involve dopant clustering. The μ_{eff} for the Co^{2+}:TiO_2 nanorods, 4.15 μ_B/Co^{2+}, is in close agreement with that obtained on the isolated spherical nanocrystals (4.2 μ_B/Co^{2+})[12] and is consistent with high-spin Co^{2+} in a low-symmetry split $^4T_1$ (^4E, D_{2d}) ground state. Surface-capped Co^{2+}:TiO_2 and Cr^{3+}:TiO_2 nanorods are therefore quantitatively paramagnetic, showing no evidence of superparamagnetism or ferromagnetism.

IV.C. Activating Ferromagnetism. We now consider the three hypotheses for ferromagnetic activation described in the Introduction.

IV.C.i. Domain Volumes. The volumes of the ferromagnetic domains in Co^{2+}:TiO_2 films made from spherical nanocrystals (Figure 5C) can be roughly estimated by fitting the 300 K ferromagnetic saturation data to a hypothetical spin-state using the Brillouin function (eq 1). Best fits to these data (not shown) yield effective spin states of ~5000, or ~3300 Co^{2+} ions. This value is likely not very accurate, but it provides an order of magnitude estimate of the number dopants involved in the ferromagnetic domains.[23] This estimate is far too large to be consistent with ferromagnetism in individual 5 nm diameter spherical 4% Co^{2+}:TiO_2 nanocrystals, which have on average only ~80 Co^{2+} ions per particle. This comparison suggests participation of ~40 or more 4% Co^{2+}:TiO_2 nanocrystals in a single ferromagnetic domain. From the mean nanorod dimensions in Figure 1 C and D, and the mean Co^{2+} concentration (4%), an average of ~2000 Co^{2+} ions per Co^{2+}:TiO_2 nanorod is estimated. Since the number of dopants per rod is on the same order of magnitude as the number of dopants in a ferromagnetic domain, these nanorods should be sufficiently large for cooperative magnetic ordering if hypothesis (1) were correct. From the powder susceptibility of the isolated Co^{2+}:TiO_2 and Cr^{3+}:TiO_2 nanorods (Figure 4) it is clear that no cooperative magnetic effects (i.e., superparamagnetism or ferromagnetism) exist in the individual nanorods themselves. This conclusion is of primary interest to the field of spintronics since it demonstrates that successful homogeneous incorporation of transition metal dopants onto the Ti^{4+} cation sites in anatase TiO_2 is not itself sufficient to generate ferromagnetism. Additional electronic or structural factors are required. From this, we conclude that hypothesis (1) is incorrect.

IV.C.ii. Thermal Annealing. Thermal annealing has been shown to enhance ferromagnetism in a vacuum-deposited Co^{2+}:TiO_2 films[9] or to activate it in spin-coated nanocrystalline[12] or sol−gel[24] films of TM^{n+}:TiO_2. Thermal annealing under reductive conditions at elevated temperatures has also been found to cause migration of Co^{2+} within the TiO_2 matrix,[7] in some cases forming segregated precipitates.[6] To investigate the role of annealing, as well as the potential for dopant migration within the nanocrystalline host, the 4.0% Co^{2+}:TiO_2 nanorods were annealed as colloids in pure TOPO at 250, 300, and 320 °C. The highest of these temperatures is very similar to that used for the spin-coat processing, where ferromagnetism was

(19) Figgis, B. N.; Hitchman, M. A. *Ligand Field Theory and its Applications*; Wiley: New York, 2000.
(20) Ikebe, M.; Miyako, Y.; Date, M. *Jpn. J. Appl. Phys.* **1969**, *26*, 43.
(21) Bendix, J. *LIGFIELD*, version 0.8x; Copenhagen, Denmark, 1994.
(22) Lever, A. B. P. *Inorganic Electronic Spectroscopy*, 2nd ed.; Elsevier Science Publishers: Amsterdam, 1984; Rahman, H. U. *J. Nat. Sci. Math.* **2000**, *40*, 1.

(23) For comparison, ferromagnetic x% Co^{2+}:TiO_2 anatase islands have been prepared by OPA-MBE.[7] The smallest of these ferromagnetic islands are ~44 nm in diameter and 7 nm in height and have $x = 5$, from which the domains are estimated to contain ~15 000 Co^{2+} ions.

(24) Suryanarayanan, R.; Naik, V. M.; Kharel, P.; Talagala, P.; Naik, R. *J. Phys.: Condens. Matter* **2005**, *17*, 755.

observed. If Co^{2+} ions were mobile in TiO_2 at these temperatures, Co^{2+} migration to the nanocrystalline surfaces would occur readily since the distance from the center of a ~6 nm diameter nanorod to the surface is less than only 8 unit cells. Once at the surface, rapid TOPO ligand exchange would occur, removing the Co^{2+} from the surface as demonstrated previously.[12,25−27] The constant Co^{2+} concentration observed during these experiments even over extended anneal times (Figure 6, up to 40 h anneal times) strongly argues that transition metal dopants are not mobile in the anatase host lattice under the conditions used for the spin coat processing (350 °C, ≤3 min anneal times) to activate ferromagnetism. The absence of ferromagnetism after colloid annealing (Figure 7) indicates that thermal migration of oxygen vacancies or other defects is also not the key requirement for ferromagnetism.

To determine whether these Co^{2+}:TiO_2 nanorods were fundamentally changed by colloidal annealing, films of the annealed nanorods were prepared by spin coating as described above. The resulting ferromagnetic saturation moments agreed well with those obtained from unannealed Co^{2+}:TiO_2 nanorods (Figure 5A, see the Supporting Information). This result demonstrates that colloid annealing did not alter the nanorods themselves in any way that would prohibit activation of ferromagnetism during the spin-coating procedure and also indicates that the paramagnetic-to-ferromagnetic activation mechanism is not critically dependent upon the identity of the surface-capping ligand (OA vs TOPO, see ref 28). Combined, these experiments show that thermal annealing alone does not activate ferromagnetism and that hypothesis (2) is thereby incorrect.

IV.C.iii. Interfacial Fusion Defects. Donor type defects such as oxygen vacancies, O_v^{n-}, have been proposed to be key elements necessary for ferromagnetism in transition metal-doped TiO_2.[10,11,14] Correlations between conductivity (presumably due to O_v^{n-}) and ferromagnetism have been reported,[11] although a recent report on highly insulating Co^{2+}:TiO_2 has suggested that O_v^{n-} at some unknown concentration may yield ferromagnetism without electrical conductivity.[9] Aerobic aggregation has been shown to activate high-T_C ferromagnetism in nanocrystals of doped ZnO DMSs[26,29] through the generation of n-type defects at interfacial fusion boundaries between adjacent nanocrystals. The possibility that ferromagnetism in TM^{n+}:TiO_2 is also activated by the introduction of donor type defects upon aggregation has been tested using low-temperature aggregation of Co^{2+}:TiO_2 nanorods and nanocrystals in the absence of surface protecting groups. Though weak, a 300 K ferromagnetic saturation moment is readily observed in the aggregated Co^{2+}:TiO_2 nanorods, and a larger moment is observed in aggregated Co^{2+}:TiO_2 nanocrystals (Figure 7). From these data, we conclude that the primary mechanism for ferromagnetic activation in our Co^{2+}:TiO_2 samples is interfacial defect formation during nanocrystal aggregation and, hence, that hypothesis (3) is correct.

Insight into the identity of the defects generated in nanocrystalline TiO_2 aggregates and spin-coated films can be gained by considering the chemical composition of the nanocrystalline surfaces prior to aggregation. Oleic acid has been shown to coordinate to TiO_2 nanorods by a chelating bidentate interaction of the $-COO^-$ group to a Ti^{4+}-rich surface.[15] Upon aggregation, this metal-rich surface presents a deficiency of lattice O^{2-} ions, leading to a concentration of charged oxygen vacancies (O_v^{n-}) at the nanocrystalline fusion interfaces.[30] We propose that the generation of interfacial O_v^{n-} is the key microscopic perturbation occurring during aggregation that transforms paramagnetic TM^{n+}:TiO_2 ($TM^{2+} = Co^{2+}$ or Cr^{3+}) into its ferromagnetic phase.

Aerobic spin coating and annealing activates ferromagnetism in Co^{2+}:TiO_2 nanorods to yield M_s(300 K) values several orders magnitude larger than those observed upon passive aggregation (0.069 vs 0.0003 μ_B/Co^{2+}). This enhancement is attributed to a greater concentration of interfacial defects created during the rapid thermal annealing of the spin-coating process than are formed by passive low-temperature aggregation. The importance of interfacial defects is apparent from the fact that the average 300 K saturation moment for spin-coated films prepared from nanocrystals is ~14 times greater than that for films made from nanorods of nearly equivalent composition (3% Co^{2+}:TiO_2, 1.0 vs 0.069 μ_B/Co^{2+}), with the highest moment (M_s(300 K) = 1.9 μ_B/Co^{2+}) exceeding those grown by vacuum deposition methods. This trend is also observed in the 25 °C aggregation experiments (Figure 6, M_s(300 K) = 0.0015 (nanocrystals) vs 0.0003 μ_B/Co^{2+} (nanorods)) and appears to be general for these oxide DMSs. The greater saturation moments found for films made from nanocrystals than from nanorods can be directly related to their different surface area/volume (SA/vol) ratios. For instance, a 6 nm × 56 nm nanorod (Figure 1) has a SA/vol ratio of ~0.67 nm^{-1}, while a 5 nm diameter spherical nanocrystal has a SA/vol of ~1.2 nm^{-1}. The greater SA/vol ratio of the nanocrystals increases the probability of forming interfacial defects (per unit volume), resulting in greater M_s values. The nanocrystals also have a larger fraction of higher surface free energy (001) facets[16] per unit volume than the nanorods, which may promote the formation of high-energy grain boundary defects upon interfacial fusion. It is this difference in surface free energy between the (101) and (001) facets that gives rise to the anisotropic growth of the nanorods (Figures 1 and 2).

Figure 8 shows that in addition to surface area, the magnitude of M_s can be controlled by the time that the spin-coated film is annealed under aerobic conditions. Given the association of activated ferromagnetism with interfacial fusion defects, the initial rise in M_s(300 K) is attributed to the formation of fusion defects, whereas its decline at longer times is attributed to passivation of these defects, most likely by atmospheric oxygen or water from the aerobic annealing environment. This conclusion is supported by the decreasing electrical conductance in nanocrystalline TiO_2 (rutile) thin films observed with aerobic annealing under conditions very similar to those used here, also attributed to the passivation of electrically active O_v^{n-} shallow donors.[31] We therefore conclude that high-T_C ferromagnetism is an intrinsic property of the nonstoichiometric DMSs TM^{n+}:$TiO_{2-\delta}$ ($TM^{n+} = Co^{2+}$ or Cr^{3+}), which are themselves extrinsic semiconductors.

The proposed activation/deactivation process is summarized in Scheme 1. As shown in Figures 4 and 7, surface-passivated

(25) Norberg, N. S.; Kittilstved, K. R.; Amonette, J. E.; Kukkadapu, R. K.; Schwartz, D. A.; Gamelin, D. R. *J. Am. Chem. Soc.* **2004**, *126*, 9387.
(26) Schwartz, D. A.; Norberg, N. S.; Nguyen, Q. P.; Parker, J. M.; Gamelin, D. R. *J. Am. Chem.* Soc. **2003**, *125*, 13205.
(27) Schwartz, D. A.; Kittilstved, K. R.; Gamelin, D. R. *Appl. Phys. Lett.* **2004**, *85*, 1395.
(28) Kittilstved, K. R.; Gamelin, D. R. *J. Am. Chem. Soc.* **2005**, *127*, 5292.
(29) Radovanovic, P. V.; Gamelin, D. R. *Phys. Rev. Lett.* **2003**, *91*, 157202.
(30) Kofstad, P. *Nonstoichiometry, Diffusion, and Electrical Conductivity in Binary Metal Oxides*; Wiley: New York, 1972.
(31) Rothschild, A.; Komem, Y.; Cosandey, F. *Interface Sci.* **2002**, *9*, 157.

Scheme 1

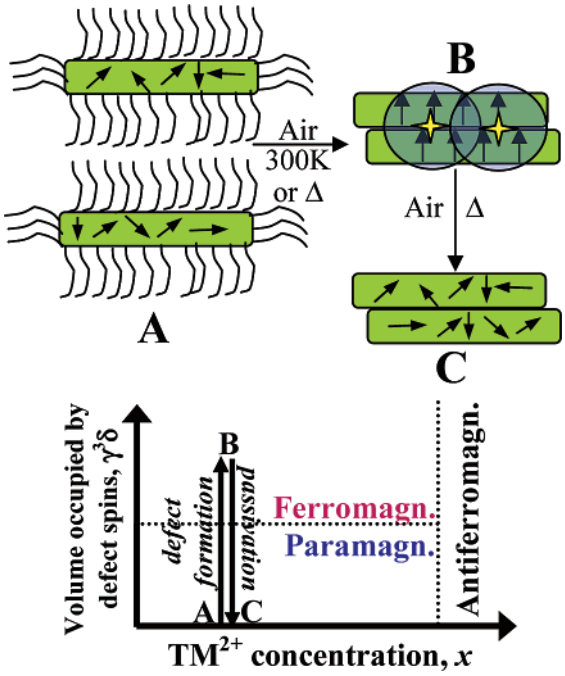

TM^{n+}:TiO_2 nanorods are paramagnetic (A), lacking the necessary defects capable of mediating ferromagnetism. The spin-coating/annealing process creates interfacial defects whose radii are sufficiently large to overlap many dopant ions as well as adjacent defects, causing a net alignment of the dopant spins following the bound magnetic polaron (BMP) mechanism (B).[14,32] This conclusion is supported by the data in Figures 5, 7, and 8. Additional aerobic heating passivates the interfacial defects, returning the sintered ferromagnetic nanorods to their paramagnetic phase (C). The lower part of Scheme 1 shows a magnetic phase diagram (adapted from ref 14) in which the volumetric extent of the defect hydrogenic wave function, γ^3, multiplied by the nonstoichiometric defect concentration, δ, is plotted versus the dopant concentration, x. Since γ^3 is constant for a given defect and x is constant for samples made from the same batch of precursors, the only parameter varied in the annealing experiments of Figure 8 is δ. By changing δ through defect formation and passivation, the ferromagnetism is controllably turned on and then off again with no other changes in materials structure or composition. To our knowledge, this is the only mechanistic study to date in which TM^{n+}:TiO_2 DMS ferromagnetism has been activated and deactivated at sufficiently low temperature to rule out dopant migration in the host lattice. These results are consistent with the general donor-mediated BMP exchange mechanism,[14,32] and additionally provide new microscopic information about the identities of the activating donor defects.

Recently, grain boundary defects at nanocrystalline fusion interfaces have been suggested to be critical components of ferromagnetism in Co^{2+}- and Ni^{2+}-doped ZnO[26,27,29] and in Ni^{2+}-doped SnO_2.[33] The conclusion here that a similar phenomenon also occurs in both Co^{2+}:TiO_2 and Cr^{3+}:TiO_2 suggests that grain boundary defects may be more generally important in regulating the ferromagnetism of oxide DMSs than is currently appreciated. For example, thin film/substrate interfaces have been suggested to be a source of ferromagnetism TM/SnO_2 (TM = Mn, Co, Fe),[14] but ferromagnetism is not actually observed in this same lattice without magnetic dopants. Similarly, saturation moments of chromium-doped SnO_2 thin films reportedly vary by over a factor of 20 depending on the identity of the substrate ($LaAlO_3$ versus $SrTiO_3$), despite the absence of significant differences in epitaxial strain (evidenced by lattice parameters).[34] Our data suggest that in these cases, too, charged grain boundary (or analogous) defects may play important roles as activators of ferromagnetic transition metal exchange coupling. As such, the critical roles played by these lattice defects may likely be responsible for some of the confusing disparities in magnetism that have been reported for otherwise seemingly identical oxide diluted magnetic semiconductors.[13,14]

V. Conclusion

The central conclusion of this study is that crystalline domain size, thermal annealing, and dopant or defect migration are not the dominating factors contributing to the conversion of doped TiO_2 nanocrystals from the paramagnetic state to the ferromagnetic state. The most important factor for activating ferromagnetism in nanocrystalline TM^{n+}:TiO_2 (TM^{n+} = Co^{2+} or Cr^{3+}) is the creation of grain boundary defects, proposed to be oxygen vacancies at nanocrystal fusion interfaces. These defects are passivated and the ferromagnetism destroyed by further aerobic annealing. We emphasize that these experiments were all performed at temperatures well below those causing dopant migration in TiO_2. The results presented in this study provide new insights into the microscopic origins of high-T_C TM^{n+}:TiO_2 DMS ferromagnetism, drawing particular attention to the general importance of nonstoichiometric grain boundary defects in this class of materials. Finally, these results suggest approaches to manipulating high-T_C DMS ferromagnetism using external chemical perturbations that will help guide experiments aimed at introducing appropriate defects into colloidal TiO_2 DMSs in order to form ferromagnetic DMS colloids suitable for nanospintronics applications.

Acknowledgment. Financial support from the NSF (DMR-0239325 and ECS-0224138), Research Corporation, ACS-PRF (AEF-39844), the Dreyfus Foundation, and the NNIN-REU Program are gratefully acknowledged. TEM data were collected at the University of Washington and at EMSL (PNNL), a national scientific user facility sponsored by the DOE. Dr. Chongmin Wang (PNNL) and Yuping Bao (UW) are thanked for valuable TEM assistance. The authors thank Dr. Chris Tonzola for assistance with TGA experiments and Professor Jesper Bendix (University of Copenhagen) for generously providing the LIGFIELD software used to calculate the energies of Figure 3B. D.R.G. is a Cottrell Scholar of the Research Corporation.

Supporting Information Available: Four figures showing additional electronic absorption, magnetic, and thermogravimetric data. This material is available free of charge via the Internet at http://pubs.acs.org.

JA0543447

(32) Kaminski, A.; Das Sarma, S. *Phys. Rev. Lett.* **2002**, *88*, 247202.
(33) Archer, P. I.; Radovanovic, P. V.; Heald, S. M.; Gamelin, D. R. *J. Am. Chem. Soc.* **2005**, *127*, in press.
(34) Hong, N. H.; Sakai, J.; Prellier, W.; Hassini, A. *J. Phys.: Condens. Matter* **2005**, *17*, 1697.